2012 International Conference on Indoor Positioning and Indoor Navigation, 13-15th November 2012

A Constraint Approach for UWB and PDR Fusion

Francisco Zampella*, Alessio De Angelis†, Isaac Skog†, Dave Zachariah† and Antonio Jiménez*
*Centre for Automation and Robotics (CAR),
Consejo Superior de Investigaciones Científicas (CSIC)-UPM
Ctra Campo Real km. 0.2, La Poveda, Madrid 28500, España
{francisco.zampella, antonio.jimenez}@csic.es
Web: http://www.car.upm-csic.es/lopsi
†Signal Processing Lab, ACCESS Linnaeus Centre,
KTH Royal Institute of Technology
Stockholm, Sweden
{alessio.deangelis, isaac.skog, dave.zachariah}@ee.kth.se

***Abstract*—Pedestrian Dead-Reckoning (PDR) and Radio Frequency (RF) ranging/positioning are complementary techniques for position estimation but they usually locate different points in the body (RF in the head/hand and PDR in the foot). We propose to fuse the information from both navigation points using a constraint filter with an upper bound in the distance between the estimated positions of both sensors.**

For a pedestrian with an IMU for PDR in the foot and a RF positioning system in the head, the simplest bound is a maximal distance of 2 m between the positions of the sensors, this establish a spherical limit to the difference in the positions. It is also possible to use a smaller, non-symmetrical bound that establishes an ellipsoid as the limit and improves the fusion. We propose the use of a grid of particles to approximate the mean and covariance of the states.

We have tested the algorithm by processing data from an Ultra Wide Band (UWB) positioning sensor attached to an IMU, both placed on the helmet of a person, and a foot-mounted IMU. Our results show that the system is able to estimate the position of a person with a limited error growth for the dead reckoning system and a better position estimate between position updates for the UWB system.

***Index Terms*—Pedestrian Dead-Reckoning, Ultra Wide Band, nonlinear constraints, sensor fusion, zero-velocity detection**

I. Introduction

The field of indoor positioning has experienced great interest in the recent years due to the market of location based services and the development of new technologies. The improvements in Micro Electro Mechanical (MEM) devices have allowed a person to use sensors previously too expensive or heavy to be carried by a pedestrian like an Inertial Measurement Unit (IMU). The inertial sensors assist in the estimation of the position of other sensors, but due to the amount of noise and bias presented in a MEM IMU, they can only propagate the position for a few seconds because the standard deviation of the position error grows with the cubic time [1].

A common technique to reduce the error growth is the Pedestrian Dead-Reckoning (PDR, [2], [3], [4]), that places an IMU in the foot and uses Zero velocity UPdaTes (ZUPT) during the stance phase to estimate and correct the errors of the navigation states in an Extended Kalman filter (EKF). In [5] the changes in the measured magnetic fields are used to estimate the turn rate of the sensor and therefore limit the grow of the orientation, but this technique requires a magnetometer that is not always available. Although PDR produces a good relative positioning and a high sampling rate, the standard deviation of the position error grows linearly with time and therefore it should use additional information to bound the error growth.

Another solution to the positioning problem relies on the existence of a network of beacons placed in known positions of the building. Using the distances or angles to the beacons, it is possible to estimate the position of a person, these techniques are called Local Positioning Systems (LPS). The angle or distances to the known points can be obtained using cameras, ultrasound or Radio Frequency (RF) systems [6]. The latter are preferred due to their range of usage and popularization in wireless communication, among those technologies we will focus on Ultra Wide Band (UWB) systems [7] due to their precision. Usually LPS systems are able to provide the global positioning with a limited error, but they require a line of sight with the beacons and usually have a low sampling rate. In many cases an IMU is used to increase the sampling rate of the system and provides a measurement of the system dynamics [8], diminishing the error of the system.

Both solutions are complementary, but in most cases they can not be integrated directly in one sensor due to the fact that PDR needs to place the IMU in the foot, and LPS systems require the antennas to be placed in the upper part of the body for a better line of sight. If the IMU and the RF antenna are both placed in a laptop [9] the IMU does not have good zero velocity updates and might diverge quickly. If both sensors are in the foot [10] the antenna might have a bad line of sight and will generate a significant amount of outliers. Other techniques use the IMU in the foot and the antenna in another part of the body [11], [12], and increase the covariance of the measurement to account for the unknown relative position between navigation points. Other authors [13], [14] use a model of the lever arm but as the real relative position is not known, this might affect the dynamics of the navigation points.

As a way of fusing the information from two sensors, we will study the positions of the navigation points during normal walk and establish a limited distance constraint in the probability density function of the relative distance between the points as a way to relate the IMU on the foot and an antenna in the head/chest. The limited distance constraint can

978-1-4673-1954-6/12/$31.00

be expressed as a quadratic inequality [15], [16], [17] that bounds the probability distribution. In section II we study the constraint filter and propose the use of a particle filter to calculate the propagation of the mean and covariance of the propagated states. In Section III we discuss the platform used and in Section IV the system is tested using an IMU with an UWB system in the head and an IMU in the foot for PDR. Conclusions are presented in Section V.

II. Constraint filter

The Kalman filters have shown to be an excellent way of fusing information for state estimation, but many non linear conditions can't be handled by it. Among those conditions we encounter the inequality constraints [17], that limits the values of some probability distributions. The inequality constraints can be used to take advantage of the fact that if we have two navigation points in the body they will have a limited distance between them and we will show that it limits the growth of the error in the systems.

Assuming we have two navigation points, $X^1 = [(r^1)^T, (X_o^1)^T]^T$ and $X^2 = [(r^2)^T, (X_o^2)^T]^T$, where $r^{(i)}$ is the position and $X_o^{(i)}$ are the other m_i navigation states of the i-th navigation point. Without a known relative position $\Delta X = X^1 - X^2$, the estimation generates two independent problems and it does not allows a direct information fusion. If both sensors are on the body of a person, it is possible to assume that there is a limited distance between the points and it might help to reduce the system error covariance. In [15], [16], [17] the effect of establishing a bound in the joint states $X = [(X^1)^T, (X^2)^T]^T$ ($n = m_1 + m_2 + 6$ states) is treated as the inequality:

$$\|L \cdot X\| \leq \gamma. \tag{1}$$

Choosing L for $L \cdot X = r^1 - r^2 = \Delta r$, is a way to limit the maximal distance between navigation points to a sphere of radius γ, but other shapes can be implemented as the ellipsoid:

$$L \cdot X = \begin{bmatrix} (r_x^1 - r_x^2)/d_1 \\ (r_y^1 - r_y^2)/d_2 \\ (r_z^1 - r_z^2)/d_3 \end{bmatrix}, \tag{2}$$

where $r_i^{(j)}$ is the component in the axis $i = \{x, y, z\}$ of the navigation point j, and d_i is the limit of the ellipsoid in the axis i.

Obtaining a new mean and covariance of the states can be treated in several ways, in [17] several methods are presented for treating the condition in (1), among them we will treat the projection and the truncation of the probability density function. After the proposed method we will introduce an approximation method for calculating the mean and covariance of the states.

A. Projection methods

In [17] the problem is treated as an "Estimate projection" for Gaussian distributions, where the new mean $\hat{X}^+$ is obtained from the minimization of a weighted distance between the constrained values and the estimated mean $\hat{X}^+$. The constrained estimate can be written as:

$$\tilde{X}^+ = \text{argmin}_X (X - \hat{X}^+)^T \cdot W_c \cdot (X - \hat{X}^+), \tag{3}$$

such that (1) is true.

If the weighting factor W_c is the inverse of the estimated covariance $W_c = (P^+)^{-1}$, the obtained projection coincide with the maximal probability estimate among the constrained values, but if $W_c = I$, the identity matrix, the projection is the closest point to the estimated mean. In [18] the problem is solved using a quadratic constraint $(L \cdot X)^T \cdot (L \cdot X) \leq \gamma^2$ and an iterative method. In [16] an approximation is proposed, to obtain the covariance of the constrained states $\tilde{P}^+$ using the gradient of the projection ∇_p, as:

$$\tilde{P}^+ = \nabla_p \cdot P^+ \cdot \nabla_p^T. \tag{4}$$

This method uses the state with the maximal probability (not the mean) as the estimate, and as ∇_p is singular, the covariance is altered, therefore other methods must be studied.

B. Probability Density Function Truncation

In [19] the mean and covariance of a system constrained in one dimension is obtained using the truncation of the probability density function (pdf). This method is only valid for constraints in only one state and in our case we want to truncate the pdf simultaneously in more than one, therefore we propose to study the pdf truncation to calculate the mean and covariance of the constrained states.

If we asume the estimated pdf $p(X)$ to be Gaussian ($X \sim \mathcal{N}(\hat{X^+}, P^+)$), the pdf of the constrained state $p(X_c) = p(X|C)$ (in our case C equal to $\|L \cdot X\| \leq \gamma$) will be:

$$\begin{aligned} p(X_c) &= \frac{p(C|X) \cdot p(X)}{\int p(C|X) \cdot p(X) \mathrm{d}x}, \\ &= \begin{cases} \frac{p(X)}{\alpha} & \text{if } \|L \cdot X\| \leq \gamma, \\ 0 & \text{else} \end{cases} \end{aligned} \tag{5}$$

where α is:

$$\alpha = \int p(C|X) \cdot p(X) \mathrm{d}x = \int_{X_c^*} p(X) \mathrm{d}x \tag{6}$$

and

$$X_c^* = \{X \in \Re^n : \|L \cdot X\| \leq \gamma\} \tag{7}$$

The mean $\hat{X}_c$ and covariance P_c can be calculated as:

$$\hat{X}_c = \int_{X_c^*} X_c \cdot p(X_c) \mathrm{d}x_c \tag{8}$$

$$P_c = \int_{X_c^*} (X_c - \hat{X}_c) \cdot (X_c - \hat{X}_c)^T \cdot p(X_c) \mathrm{d}x_c \tag{9}$$

C. Integral calculation

For a pdf truncation approach, we propose to use a grid of particles to estimate the 3 integrals (6, 8 and 9). We first generate a set of N points uniformly distributed around the constrained area ($X_i \in X_c^*$) with an integration interval $\mathrm{d}x_c \approx \Delta X_i$ and assuming a Gaussian distribution, calculate its corresponding probabilities $p(X_i)$, then we can estimate α as:

$$\alpha = \sum_{i=1}^{N} p(X_i)\Delta X_i. \tag{10}$$

If we define $p'(X_i) = p(X_i)/\alpha$, then (8) and (9) can be approximated as the sums:

$$\hat{X}_c = \sum_{i=1}^{N} X_i \cdot p'(X_i)\Delta X_i \tag{11}$$

and

$$P_c = \sum_{i=1}^{N}(X_i - \hat{X}_c)(X_i - \hat{X}_c)^T p'(X_i)\Delta X_i \quad + R_c, \tag{12}$$

where R_c is a quantization noise added due to the grids.

The previous equations can be simplified calculating the value

$$\alpha' = \sum_{i=1}^{N} p(X_i). \tag{13}$$

where $\alpha = \alpha'\Delta X_i$ and defining $p^*(X_i) = p'(X_i)\Delta X_i = p(X_i)/\alpha'$, then (11) and (12) can be rewritten as:

$$\hat{X}_c = \sum_{i=1}^{N} X_i \cdot p^*(X_i) \tag{14}$$

and

$$P_c = \sum_{i=1}^{N}(X_i - \hat{X}_c)(X_i - \hat{X}_c)^T p^*(X_i) \quad + R_c, \tag{15}$$

D. State transformation

In a pdf truncation approach, the use of grids to calculate those 3 integrals (6, 8 and 9) will require a significant amount of points, therefore we intend to use a reduced state study as propose in [20]. For spherical constraints, the states can be rewritten with a linear transformation $Z = [Z_1^T, Z_2^T]^T = T \cdot X \in \Re^n$, such that $Z_1 = [r_1 - r_2]$ and $Z_2 = [X_{o,1}^T, (r_1 + r_2)^T, X_{o,2}^T]^T$, where:

$$T = \begin{bmatrix} I_3 & 0_{3\times m_1} & -I_3 & 0_{3\times m_2} \\ 0_{m_1\times 3} & I_{m_1} & 0_{m_1\times 3} & 0_{m_1\times m_2} \\ I_3 & 0_{3\times m_1} & I_3 & 0_{3\times m_2} \\ 0_{m_2\times 3} & 0_{m_2\times m_1} & 0_{m_2\times 3} & I_{m_2} \end{bmatrix} \tag{16}$$

and the constraint is reduced to $\|L \cdot T^{-1} \cdot Z\| = \|Z_1\| \leq \gamma$. For ellipsoidal constraints it is useful to use $Z_1 = L \cdot X$ (from eq. 2) and

$$Z_2 = \begin{bmatrix} X_{o,1} \\ (r_{x1} + r_{x2})/d_1 \\ (r_{y1} + r_{y2})/d_2 \\ (r_{z1} + r_{z2})/d_3 \\ X_{o,2} \end{bmatrix}. \tag{17}$$

This transformation passes the ellipsoidal constraint to an spherical constraint problem in Z.

In [20], is assumed that if X is Gaussian, Z will also have a Gaussian distribution with an estimated mean $\hat{Z} = T \cdot \hat{X}$ and covariance $P_z = T \cdot P^+ \cdot T^T$. Separating the inverse of the Covariance P_z according to the corresponding parts of Z_1 and Z_2:

$$P_z^{-1} = W = \begin{bmatrix} W_{11} & W_{12} \\ W_{12}^T & W_{22} \end{bmatrix}, \tag{18}$$

if $W'_{11} = W_{11} - W_{12}W_{22}^{-1}W_{12}^T$, we can define $p_1(Z_1)$ as:

$$p_1(Z_1) \quad = \quad \frac{\sqrt{|W'_{11}|}}{\sqrt{2\pi}^3} e^{-(\Delta Z_1^T W'_{11} \Delta Z_1)/2} \tag{19}$$

where $\Delta Z_1 = Z_1 - \hat{Z}_1$, and $\hat{Z}_1$ is the estimated mean of Z_1. We will define a normalization factor α_z as:

$$\alpha_z \quad = \quad \int_{Z_1^*} p_1(Z_1)\mathrm{d}Z_1 \tag{20}$$

where

$$Z_1^* = \{Z_1 \in \Re^3 : \|Z_1\| \leq \gamma\}. \tag{21}$$

The normalized pdf will be $p'_1(Z_1) = p_1(Z_1)/\alpha_z$ around Z_1^*. The estimated mean of the constrained distribution can be divided as $\hat{Z}_c = [\hat{Z}_{c1}^T, \hat{Z}_{c2}^T]^T$ and calculating each part [20]:

$$\hat{Z}_{c1} \quad = \quad \int_{Z_1^*} Z_1 p'_1(Z_1)\mathrm{d}Z_1, \tag{22}$$

and:

$$\hat{Z}_{c2} \quad = \quad \hat{Z}_2 - W_{22}^{-1}W_{12}^T \cdot (\hat{Z}_{c1} - \hat{Z}_1), . \tag{23}$$

The covariance of the constrained distribution can be separated in each component according to Z_1 and Z_2 as:

$$P_{zc} = \begin{bmatrix} P_{c11} & P_{c12} \\ P_{c12}^T & P_{c22} \end{bmatrix} \tag{24}$$

where [20]:

$$P_{c11} = \int_{Z_1^*} (Z_1 - \hat{Z}_{c1})(Z_1 - \hat{Z}_{c1})^T p'_1(Z_1)\mathrm{d}Z_1. \tag{25}$$

$$P_{c12} = -P_{c11}W_{12}W_{22}^{-1}. \tag{26}$$

and

$$P_{c22} = W_{22}^{-1} + W_{22}^{-1}W_{12}^T P_{c11} W_{12} W_{22}^{-1} \tag{27}$$

Once $\bar{Z}_c$ and P_{zc} are obtained, the linear transformation T can be used to obtain $\hat{X}_c = T^{-1}\hat{Z}_c$ and $P_c = T^{-1}P_{zc}(T^{-1})^T$

III. Evaluation Platform

For the evaluation of this method we propose to fuse two navigation information sources, the first is a commercially available UWB system and the second is a foot-mounted INS implementation. This section will discuss the used systems and the considerations of the relative positioning among them.

A. UWB System

The UWB system considered in this paper is a commercial Real-Time Location System (RTLS), manufactured by Ubisense [21]. It is comprised of an infrastructure section, consisting of eight wired synchronized sensors mounted in fixed surveyed positions, and of a user section consisting of several active wireless tags. The sensors are able to measure the Time-Difference-Of-Arrival (TDOA) and the angle-of-arrival (AOA) of the UWB pulses transmitted by the tags, therefore providing a centralized estimate of the tags positions with an update rate of up to 10 Hz. The system is severely affected by non line of sight conditions, but we studied the problem in the central area of the system where most of the sensors were in line of sight.

The RTLS system infrastructure has been installed and calibrated in the R1 experimental space at KTH, a $12 \times 30 \times 10$ m underground old reactor hall [1]. This experimental space provides opportunity to run full scale experiments in three dimensions, since one side of the hall consists of three stories of office modules. Furthermore, due to its underground location, it provides a fully controllable RF environment.

The UWB system is intended to be used as a reference tool for the evaluation of the performance of research prototypes for pedestrian indoor navigation devices such as other radio-based systems, foot-mounted inertial navigation and vision-based solutions. Also, it enables scenario-based testing of navigation devices for user-specific applications, such as first-responder users. Finally, it provides a way to experimentally validate the accuracy requirements of such specific applications.

The results of a measurement campaign, carried out using a robotic laser total station as a ground truth reference, have shown that the raw unfiltered measurements of the UWB system provide an accuracy of 30 cm or better in large portions of the considered experimental space. Such an accuracy is acceptable for the intended purpose, even though the indoor radio propagation environment is particularly challenging, due to dense multipath conditions. Furthermore, from the measurement results, a coverage and accuracy map of the installed UWB system in the considered area has been generated, which is a useful reference for the performance assessment of other positioning systems. An extensive description and discussion of the measurement campaign can be found in [22].

A Microstrain 3DM-GX3-35 IMU with a sampling rate of 250 Hz, was attached to the UWB wireless tag, and both placed in the top of a helmet. We propose an Inertial Navigation System (INS) for this navigation point, tracking in the instant k, the Orientation as the Direction Cosine Matrix $C_{b,k}^{n(h)}$ (changes measures from the sensor frame, subindex b, to the navigation frame, subindex n), the orientation error $\Delta\Psi_k^h$ in the navigation system, the position r_k^h and the velocity $\dot{r}_k^h$. An INS in a generic point i in the body, is described by the following equations (for the specific case of the IMU with the Ubisense tag we will use $i = h$, and for the IMU in the foot we will use $i = f$):

$$C_{b,k}^{n(i)} = C_{b,k-1}^{n(i)} \cdot e^{[\omega_k^{(i)} \times]\Delta t^{(i)}} \quad (28)$$

$$\dot{r}_k^{(i)} = \dot{r}_{k-1}^{(i)} + (\hat{C}_{b,k}^{n(i)} \cdot \ddot{r}_k^{(i)} - g)\Delta t^{(i)} \quad (29)$$

$$r_k^{(i)} = r_{k-1}^{(i)} + (\dot{r}_k^{(i)} + \dot{r}_{k-1}^{(i)})\Delta t^{(i)}/2 \quad (30)$$

where $[\omega_k^{(i)} \times]$ is the skew symmetrical matrix for the turn rate, measured as $Gyr^{(i)}$ in the gyroscope, $\Delta t^{(i)}$ is the time interval (the sampling frequency of the Microstrain IMU is 250 Hz) and $\ddot{r}_k^{(i)}$ is the acceleration in the sensor, measured as $Acc^{(i)}$ in the accelerometer. For the state vector $X_k^{(i)} = [(r_k^{(i)})^T, (\dot{r}_k^{(i)})^T, (\Delta\Psi_k^{(i)})^T]^T$, the propagation of the estimated covariance $\hat{P}_k^{(i)}$ is:

$$\hat{P}_k^{(i)} = F_k^{(i)} \cdot P_{k-1}^{(i)} \cdot (F_k^{(i)})^T + Q^{(i)}, \quad (31)$$

where $Q^{(i)}$ is the process noise and $F_k^{(i)}$ is the state transition matrix,

$$F_k^{(i)} = \begin{bmatrix} I_3 & I_3 \cdot \Delta t^{(i)} & 0 \\ 0_3 & I_3 & [-C_{b,k}^{n(i)} Acc^(i) \times]\Delta t^{(i)} \\ 0_3 & 0_3 & I_3 \end{bmatrix}. \quad (32)$$

When an additional measurement $m_k^{(i)}$ is presented (the Ubisense tag can provide position updates at 10 Hz), the states $X_k^{(i)}$ can be updated from the previous estimate $\hat{X}_k^{(i)}$ and the measured value ($m_k^h = Pos_k^h$ for the UWB/IMU system) as:

$$X_k^{(i)} = \hat{X}_k^{(i)} + K_k(m_k^{(i)} - H_k^{(i)} \cdot \hat{X}_k^{(i)}) \quad (33)$$

$$P_k^{(i)} = (I - K_k^{(i)} \cdot H_k^{(i)})\hat{P}_k^{(i)}, \quad (34)$$

where $H_k^{(i)}$ is the observation matrix ($H_k^h = [I_3, 0_3, 0_3]$ for the Ubisense system) and the Kalman gain $K_k^{(i)}$ is:

$$K_k^{(i)} = \hat{P}_k^{(i)} \cdot (H_k^{(i)})^T \cdot (K_k^{(i)} \cdot \hat{P}_k^{(i)} \cdot H_k^T + R^{(i)})^{-1} \quad (35)$$

and $R^{(i)}$ is the measurement covariance. After each measurement update the orientation is corrected as:

$$C_{b,k}^{n(i)} = e^{[\Delta\Psi^{(i)} \times]} \cdot \hat{C}_{b,k}^{n(i)}, \quad (36)$$

and the orientation error is reset.

B. Foot-Mounted INS

The PDR system used in this paper is an open source embedded foot-mounted INS implementation, including both hardware and software design called OpenShoe [23]. The system is based in an Analog Devices ADIS16367 IMU

[1] More information about the KTH R1 experimental space may be found at www.r1.kth.se

(Accelerometer and Gyroscope but no Magnetometer) and an Atmel AVR32UC3C microcontroller, capable of transmitting the raw data from the IMU or a preprocessed Position, Velocity and Orientation. The IMU is placed in the heel of a boot for an easily detected stance and a more realistic zero velocity phase.

The foot-mounted INS or PDR is based in the use of an INS with the signals from an IMU in the foot of the person. Due to the nature of the inertial navigation using consumer grade IMUs, the standard deviation of the position error grows proportional to the cubic time and after just a few seconds the estimation is usually several meters wrong.

For a pedestrian with an IMU in the foot, it is possible to identify the stance phases of the walking pattern and force the velocity to be zero, and therefore limit the growth of the position error covariance. In [1] and [3] several stance detection methods and the effect on the navigation are discussed. Using an EKF it is possible to track the errors of the navigation and eliminate them, the resulting increment of the standard deviation of the position error is approximately linear with the traveled distance.

One of the main sources of error in an inertial navigation is the heading error, some authors like [2], [5] use the magnetic field to obtain information on the attitude, but in the OpenShoe, there is no magnetometer available and it becomes an unobservable state. The PDR estimation provides good relative positioning without the use of external hardware, but it requires an initialization and occasional position updates to limit the error grow.

The proposed navigation solution for the foot (index f) is based on the tracking of the estimated orientation of the foot sensor $\hat{C}_{b,k}^{n(f)}$ and the estimated states, the error of the orientation $\Delta\Psi_k^f$ in the navigation frame, the position r_k^f and the velocity $\dot{r}_k^f$. The system evolves according to (28)-(36) where $i = f$ (the sampling frequency of the OpenShoe is 825 Hz). If a stance is detected a ZUPT measurement is implemented, where the velocity is zero ($m_k^f = [0,0,0]^T$) and the observation matrix is $H_k^f = [0_3, I_3, 0_3]$.

C. Joint Navigation System

Due to the fact that the two IMUs have different sampling rates, the measurements from the head and foot are not simultaneous. We propose an asynchronous implementation, where the joint state vector is $X_k = [(X_k^f)^T, (X_k^h)^T]$. Each system is propagated when a new IMU sample is available (if only one system receives an IMU sample the other remains the same), according to (28)-(32) where the state transition matrix is:

$$F_k = \begin{cases} \begin{bmatrix} F_k^f & 0_9 \\ 0_9 & I_9 \end{bmatrix} & \text{Foot IMU sample,} \\ \begin{bmatrix} I_9 & 0_9 \\ 0_9 & F_k^h \end{bmatrix} & \text{Head IMU sample,} \\ \begin{bmatrix} F_k^f & 0_9 \\ 0_9 & F_k^h \end{bmatrix} & \text{Both IMUs samples} \end{cases}. \quad (37)$$

Similarly the process noise Q will be

$$Q = \begin{cases} \begin{bmatrix} Q^f & 0_9 \\ 0_9 & 0_9 \end{bmatrix} & \text{Foot IMU sample,} \\ \begin{bmatrix} 0_9 & 0_9 \\ 0_9 & Q^h \end{bmatrix} & \text{Head IMU sample,} \\ \begin{bmatrix} Q^f & 0_9 \\ 0_9 & Q^h \end{bmatrix} & \text{Both IMUs samples} \end{cases}. \quad (38)$$

If a stance or a Ubisense positioning is detected, the states will be updated with (33)-(36), where the measurement m_k will be:

$$m_k = \begin{cases} [0,0,0]^T & \text{ZUPT,} \\ [Pos_k^h] & \text{Ubisense position,} \\ \left[0,0,0,(Pos_k^h)^T\right]^T & \text{Both measurements} \end{cases}. \quad (39)$$

The observation matrix H_k will be:

$$H_k = \begin{cases} \begin{bmatrix} H_k^f & 0_{3\times 9} \end{bmatrix} & \text{ZUPT,} \\ \begin{bmatrix} 0_{3\times 9} & H_k^h \end{bmatrix} & \text{Ubisense position,} \\ \begin{bmatrix} H_k^f & 0_{3\times 9} \\ 0_{3\times 9} & H_k^h \end{bmatrix} & \text{Both measurements} \end{cases}. \quad (40)$$

The measurement covariance R will be:

$$R = \begin{cases} [R^f] & \text{ZUPT,} \\ [R^h] & \text{Ubisense position,} \\ \begin{bmatrix} R^f & 0_3 \\ 0_3 & R^h \end{bmatrix} & \text{Both measurements} \end{cases}. \quad (41)$$

Both systems are related only by the fact that there is a maximal distance between them and without this information a joint navigation system is equivalent to having both INS independently, but by applying the constraint, the navigation points will have a crosscorrelation and it will decrease the error growth rate. For the constraint we define the matrix L for an ellipsoidal bound:

$$L = \begin{bmatrix} I_d & 0_{3\times 6} & -I_d & 0_{3\times 6} \end{bmatrix}, \quad (42)$$

where

$$I_d = \begin{bmatrix} 1/d_1 & 0 & 0 \\ 0 & 1/d_2 & 0 \\ 0 & 0 & 1/d_3 \end{bmatrix}. \quad (43)$$

As a way to evaluate the maximal distance between the navigation points, we recorded the position of the head and feet with a camera motion capture system during a straight walk in a treadmill and a random walk in a limited area. In figure 1 it is possible to observe that the relative positions are mainly distributed around an ellipsoid centered in the point $[0, 0, 1.65]^T$ m and with a variation of around 0.2 m in the Z axis and 0.5 m in the XY plane.

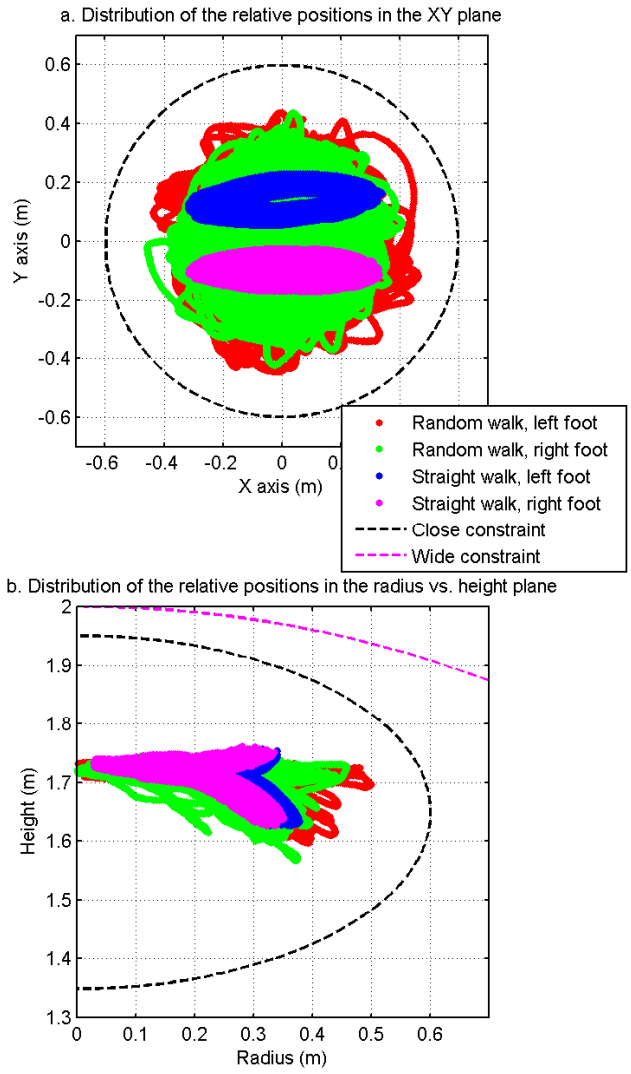

Fig. 1. Relative position of the head with respect to the foots recorded with a camera motion capture system a. Distribution in the XY plane. b. Distribution in the radius vs. height plane

We propose the use of an ellipsoidal constraint with $d_1 = 0.6$ m,$d_2 = 0.6$ m, $d_3 = 0.3$ m and $\gamma = 1$, between the head and the foot displaced to the head height as a way to limit the relative position between the foot and the head, leaving a margin for the positioning error. The foot position can be obtained subtracting the person height to r_k^f. This proposed limit uses a tighter bound that accelerates the effect of the filter.

D. UWB PDR simulation

As a way to test the behavior of the constraint and compare it with other approaches we propose a Monte Carlo simulation based on the noiseless synthetic foot positions ($r_k^{(f)}$), the corresponding IMU signals from [1] and a generated head position ($r_k^{(h)}$) and corresponding accelerations and turn rates for a pedestrian.

The signals were based in the closed loop data set proposed for the foot of a person walking 10 counterclockwise closed loops. The head is positioned at a constant height of 1.8 m and moves at an approximately constant speed, 0.1 m on the left of the path of the foot, IMU signals were obtained from the analytical representation of that position

Both points will have a maximal distance of less than 2 m, but as observed in the relative distance distribution of figure 1, the bound can be shortened to 0.6 m in the XY plane and 0.3 m in the Z axis.

The filters track the position, velocity and orientation error in both points using the IMU signals from the head and the foot (both sampled at 100 Hz and with noise recorded from a standing still IMU) and the position obtained from a simulated UWB system that provides a position measurement with Gaussian noise $Pos_k^h \sim \mathcal{N}(r_k^{(h)}, R_{\text{UWB}})$ at 5 Hz. The foot positioning is obtained using ZUPT.

The evaluated algorithms will be a reconstruction without the constraint (the upper bound), a constrained system with bounds as previously proposed and a constrained system with a bigger bound ($d_1 = 1$ m,$d_2 = 1$ m, $d_3 = 0.5$ m and $\gamma = 1$). We will observe the obtained positioning for a single case and perform a Monte Carlo simulation, executing the algorithms 100 times and adding noise to each IMU and UWB Position signal ($R_{\text{UWB}} = I_3 \cdot 1$ m^2 error). The estimated positions ($\hat{r}_k^{(f)}$ and $\hat{r}_k^{(h)}$) will be evaluated using the Root Mean Squared Errors (RMSE) of the positions.

In figure 2 the trajectory of both systems is observed without a bound in the distance, the foot position as a inertial navigation algorithm starts to accumulate heading errors that affects the positioning, while the head position presents a limited amount of error. In figure 3, by using the distance bound, both trajectories go side by side around the closed trajectory, with small fluctuations due to the measurements. The foot position keep a correct orientation and the head position appears to have less error than the unconstrained approach.

In figure 4 the evolution of the RMSE is observed for the studied methods. The unconstrained method generates the

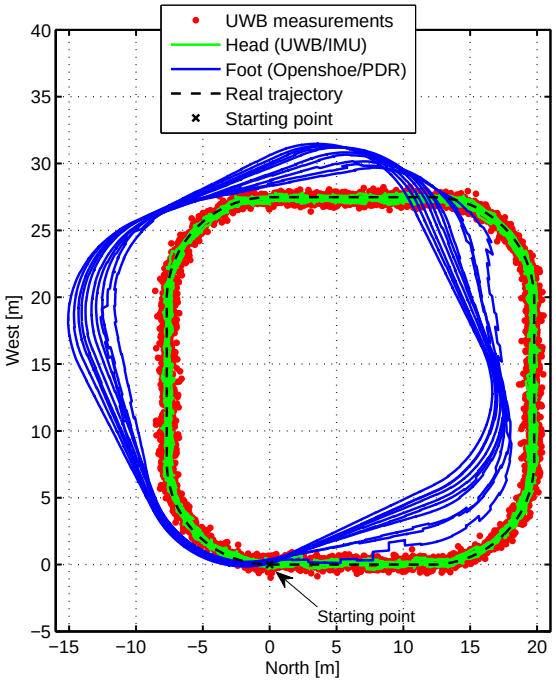

Fig. 2. Reconstruction of the position of the foot and the head without a constraint

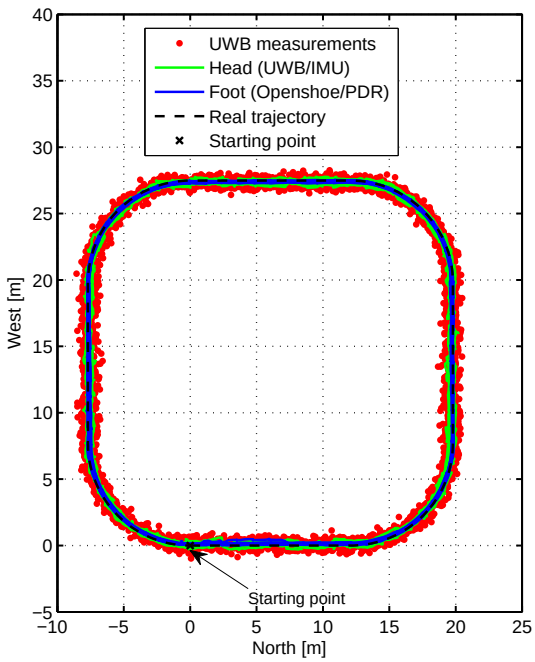

Fig. 3. Reconstruction of the position of the foot and the head with a constraint of 1 m in the XY plane and 0.5 m in the Z axis

upper bound for error growth, significantly higher due to the loss of the heading in the foot position estimation. In the case of the UWB/INS method, it reduces the error compared to the UWB alone measurements, thanks to the introduction of the IMU. The constrained approach has an even lower error growth, due mainly to the correction of the orientation in PDR. The use of tighter bounds accelerate the convergence and diminish the error for the head (UWB/INS) estimation and remains approximately the same for the foot (PDR) estimation, but if the bound is too low, the occasional points outside of the bound might affect the measurements and generate abrupt higher errors.

IV. Experimental Evaluation

For the evaluation of the system we recorded the IMUs and Ubisense positioning for a person walking counterclockwise in the R1 experimental space of KTH with a Laptop as can be observed in figure 5. An additional UWB tag was placed in the foot for an easier synchronization of the UWB and IMUs data, the position updates from this point were not used because it presented a significant amount of outliers due to a poor line of sight.

The signals of the IMU in the foot (OpenShoe) were recorded at 825 Hz, the IMU in the head had a sampling rate of 250 Hz and the update rate of the UWB tag in the head was 5 Hz. Both IMUs shared the laptop's CPU time frame, the UWB tags in the head and in the foot shared the same UWB system time frame. All the measurements were manually converted, off-line, to a common time frame matching the motion of the foot perceived from the UWB and with the PDR.

For the experiment the test subject walked 10 counterclockwise loops in an octogonal shape pattern of approximately 8.5 m by 9 m around the central area of the R1 experimental space at KTH. Figure 6 shows the independent position reconstruction of the UWB and the PDR system, a constant noisy positioning can be observed in the first and the accumulation of error produced by the heading in the second, due to the lack of an initial yaw value for the foot navigation point.

Figure 7 shows the position reconstruction using the constraint in the distance between the UWB/IMU in the head and the PDR system in the foot. Due to the unknown initial heading, the movement starts with a wrong path, but it start correcting the yaw and after some steps converges with the correct path.

The constraint filter allows a correct adjustment in situations were two navigation points are presented, one with a bounded error and another with a incrementing error, but with a good relative positioning. The cost of the constraint filter is the computation time required to estimate the mean and covariance of the bounded pdf, but with a 100 Hz IMU signal, it can calculate the position in real time. Due to the non Gaussian Position error, the constraint filter has a slightly worst effect than in the simulations, however it is able to correct wrong orientations and diminish the errors in each system.

We have observed that if the standard deviation of the position measurement updates is higher than the bounded

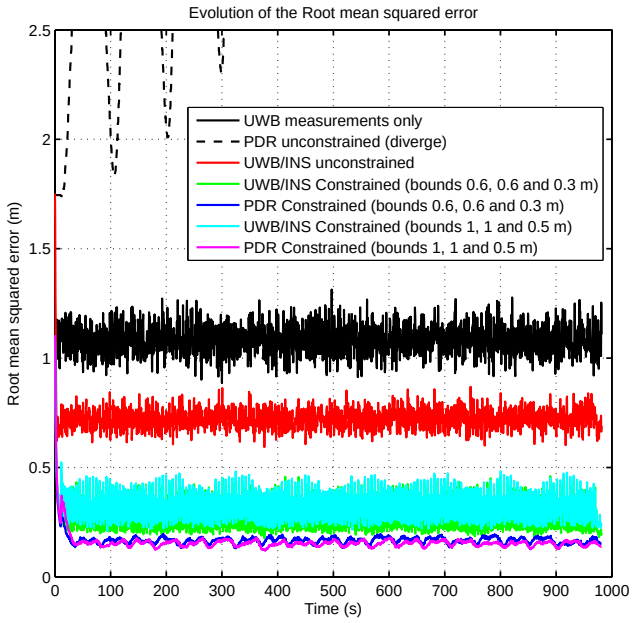

Fig. 4. Evolution of the Root Mean Squared Errors (RMSE) for the different methods studied

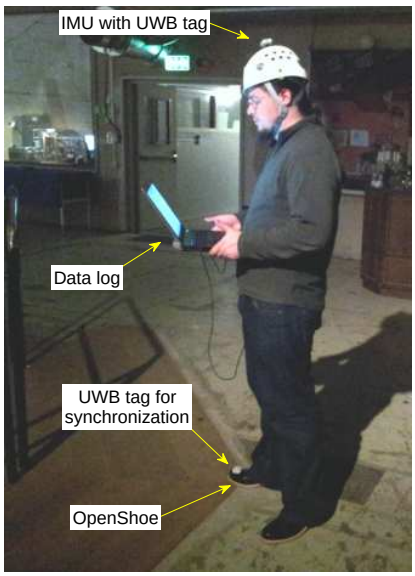

Fig. 5. Equip used during the evaluation of the system

region, the single navigation point with position updates has the same performance than the constraint filter and due to the computation time, it is preferable.

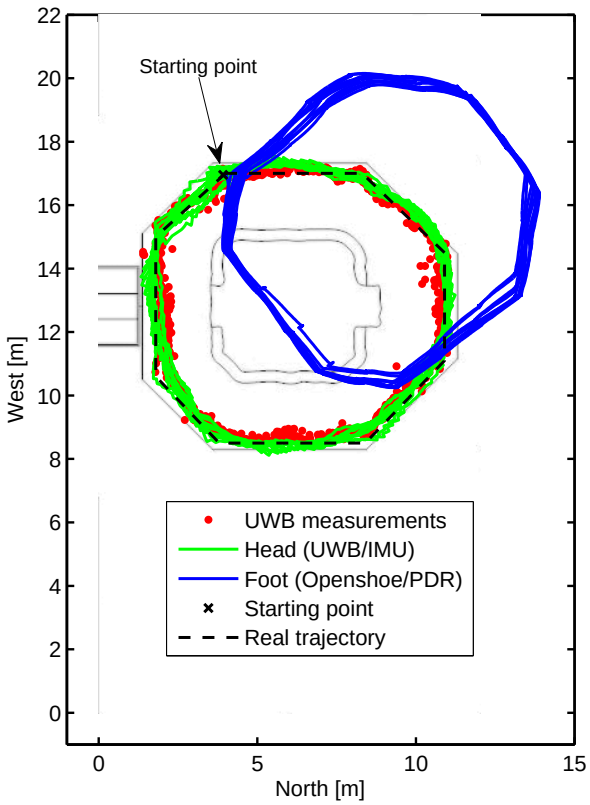

Fig. 6. Independent reconstruction of the position for an IMU in the head with UWB position measurements and an IMU in the foot with ZUPT measurements

V. Conclusions

We have presented a method for improving the estimation of two navigation points with the information that there is a maximal distance between them. The method is based on a constraint filter, which truncates the pdf of the relative position according to the established bound and estimates a new mean and covariance for the joint system.

The use of the constraint filter bounds the positioning error of a PDR estimation with respect to another positioning system, in our case UWB. In the lack of position updates, the filter lower the error growth of the UWB/INS system (approximately quadratic with time) to that of a PDR (linear with the traveled distance).

The constraint filter using a pdf truncation offers a way of propagating the statistics of the navigation states, but requires many calculations for the approximations of the truncated pdf mean and covariances. The state transformation used offers a faster method for their calculation and permits the use of a denser grid. Future work should include ways to reduce the calculation time of this approximations, better models for the truncated pdf, taking into account the non-line-of-sight

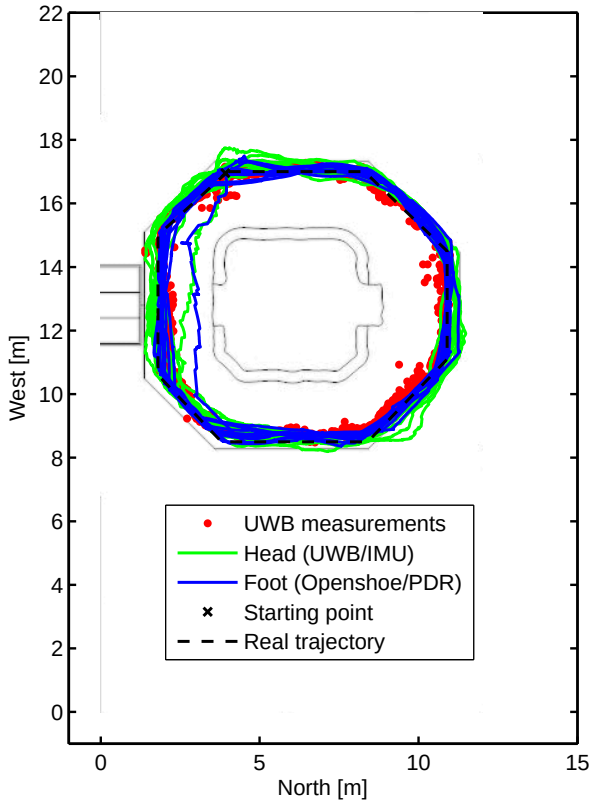

Fig. 7. Reconstruction of the position for an IMU in the head with UWB position measurements and an IMU in the foot with ZUPT measurements and a bound between the distance of both systems

conditions and the comparison of the effect of this fusion with several LPS systems or PDR systems.

Acknowledgment

This work was supported by the LEMUR project (TIN2009-14114-C04-03), LAZARO project (CSIC-PIE Ref.201150E039), JAE PREDoc scholarship, the Royal Institute of Technology (KTH) and the Swedish Agency for Innovation Systems (VINNOVA). We would like to thank the CSIC for financing the research visit that promoted this work and the Signal Processing Lab for receiving me.

References

[1] F. Zampella, A. Jimenez, F. Seco, J. Prieto, and J. Guevara, "Simulation of foot-mounted IMU signals for the evaluation of PDR algorithms," in *Indoor Positioning and Indoor Navigation (IPIN), 2011 International Conference on*, pp. 1 –7, sept. 2011.

[2] A. Jimenez, F. Seco, J. Prieto, and J. Guevara, "A comparison of Pedestrian Dead-Reckoning algorithms using a low-cost MEMS IMU," in *2009 IEEE International Symposium on Intelligent Signal Processing*, pp. 37–42, Ieee, Aug. 2009.

[3] I. Skog, P. Handel, J. Nilsson, and J. Rantakokko, "Zero-velocity detection - an algorithm evaluation," *Biomedical Engineering, IEEE Transactions on*, vol. 57, pp. 2657 –2666, nov. 2010.

[4] J. Borenstein, "Personal Dead-reckoning (PDR) System for Firefighters," in *Precision Indoor Personnel Location and Tracking for Emergency Responders, Worcester, MA, August 2-3, 2010*, p. 13, 2010.

[5] F. Zampella, M. Khider, P. Robertson, and A. Jimenez, "Unscented Kalman filter and Magnetic Angular Rate Update (MARU) for an improved Pedestrian Dead-Reckoning," in *Position Location and Navigation Symposium (PLANS), 2012 IEEE/ION*, pp. 129 –139, april 2012.

[6] F. Seco, C. Plagemann, A. Jiménez, and W. Burgard, "Improving RFID-Based Indoor Positioning Accuracy Using Gaussian Processes," in *International Conference on Indoor Positioning and Indoor Navigation*, pp. 15–17, 2010.

[7] A. De Angelis, M. Dionigi, A. Moschitta, and P. Carbone, "A low-cost ultra-wideband indoor ranging system," *Instrumentation and Measurement, IEEE Transactions on*, vol. 58, pp. 3935 –3942, dec. 2009.

[8] A. De Angelis, J. O. Nilsson, I. Skog, P. Händel, and P. Carbone, "Indoor positioning by ultra wide band radio aided inertial navigation," *Metrology and Measurement Systems*, vol. 17, no. 3, pp. 447–460, 2010. QC 20110204.

[9] P. Kemppi, T. Rautiainen, V. Ranki, F. Belloni, and J. Pajunen, "Hybrid positioning system combining angle- based localization , pedestrian dead reckoning and map filtering," in *International Conference on Indoor Positioning and Indoor Navigation*, pp. 15–17, September 2010.

[10] S. House, S. Connell, I. Milligan, D. Austin, T. Hayes, and P. Chiang, "Indoor localization using pedestrian dead reckoning updated with rfid-based fiducials," in *Engineering in Medicine and Biology Society,EMBC, 2011 Annual International Conference of the IEEE*, pp. 7598 –7601, 30 2011-sept. 3 2011.

[11] J. Rantakokko, J. Rydell, P. Stromback, P. Handel, J. Callmer, D. Tornqvist, F. Gustafsson, M. Jobs, and M. Gruden, "Accurate and reliable soldier and first responder indoor positioning: multisensor systems and cooperative localization," *Wireless Communications, IEEE*, vol. 18, pp. 10 –18, april 2011.

[12] A. Jimenez Ruiz, F. Seco Granja, J. Prieto Honorato, and J. Guevara Rosas, "Accurate pedestrian indoor navigation by tightly coupling foot-mounted imu and rfid measurements," *Instrumentation and Measurement, IEEE Transactions on*, vol. 61, pp. 178 –189, jan. 2012.

[13] J. B. Bancroft and G. Lachapelle, "Data fusion algorithms for multiple inertial measurement units," *Sensors*, vol. 11, no. 7, pp. 6771–6798, 2011.

[14] J. Pinchin, C. Hide, K. Abdulrahim, T. Moore, and C. Hill, "Integration of Heading-Aided MEMS IMU with GPS for Pedestrian Navigation," *Proceedings of the 24th International Technical Meeting of The Satellite Division of the Institute of Navigation (ION GNSS 2011)*, p. 1346, September 2011.

[15] D. Simon and T. L. Chia, "Kalman filtering with state equality constraints," *Aerospace and Electronic Systems, IEEE Transactions on*, vol. 38, pp. 128 –136, jan 2002.

[16] S. Julier and J. LaViola, "On kalman filtering with nonlinear equality constraints," *Signal Processing, IEEE Transactions on*, vol. 55, pp. 2774 –2784, june 2007.

[17] D. Simon, "Kalman filtering with state constraints: a survey of linear and nonlinear algorithms," *Control Theory Applications, IET*, vol. 4, pp. 1303 –1318, august 2010.

[18] C. Yang and E. Blasch, "Kalman filtering with nonlinear state constraints," *Aerospace and Electronic Systems, IEEE Transactions on*, vol. 45, pp. 70 –84, jan. 2009.

[19] D. Simon and D. L. Simon, "Constrained kalman filtering via density function truncation for turbofan engine health estimation," *Intern. J. Syst. Sci.*, vol. 41, pp. 159–171, Feb. 2010.

[20] D. Zachariah, I. Skog, M. Jansson, and P. Hndel, "Bayesian estimation with distance bounds," in *IEEE Signal Processing Letters (Accepted for publication)*, 2012.

[21] Ubisense Ltd., *The Ubisense Precise Real-time Location System - Series 7000 Sensor*, 2011.

[22] A. De Angelis, P. Händel, and J. Rantakokko, "Measurement report. Laser total station campaign in KTH R1 for Ubisense system accuracy evaluation," tech. rep., KTH, Signal Processing, 2012. (Technical Report) QC 20120618 [Online]. Available: http://urn.kb.se/resolve?urn=urn:nbn:se:kth:diva-98046.

[23] J.-O. Nilsson, I. Skog, P. Handel, and K. Hari, "Foot-mounted INS for everybody - an open-source embedded implementation," in *Position Location and Navigation Symposium (PLANS), 2012 IEEE/ION*, pp. 140 –145, april 2012.